High-Pressure Synthesis, Crystal Structure, and Electromagnetic Properties of CdRh$_2$O$_4$: an Analogous Oxide of the Postspinel Mineral MgAl$_2$O$_4$

Xia Wang,[†,‡] Yanfeng Guo,[*,‡] Youguo Shi,[§] Alexei A. Belik,[∥] Yoshihiro Tsujimoto,[∥] Wei Yi,[∥] Ying Sun,[∥] Yuichi Shirako,[⊥] Masao Arai,[⊗] Masaki Akaogi,[⊥] Yoshitaka Matsushita,[○] and Kazunari Yamaura[*,†,‡]

[†]Department of Chemistry, Graduate School of Science, Hokkaido University, Sapporo, Hokkaido 060-0810, Japan

[‡]Superconducting Properties Unit, [∥]International Center for Materials Nanoarchitectonics (WPI-MANA), and [⊗]Computational Materials Science Unit, National Institute for Materials Science, 1-1 Namiki, Tsukuba, Ibaraki 305-0044, Japan

[§]Institute of Physics, Chinese Academy of Sciences, Beijing 100190, China

[⊥]Department of Chemistry, Gakushuin University, 1-5-1 Mejiro, Toshima-ku, Tokyo 171-8588, Japan

[○]Synchrotron X-ray Station at SPring-8, National Institute for Materials Science, 1-1-1 Kouto, Sayo-cho, Hyogo 679-5148, Japan

ⓢ *Supporting Information*

ABSTRACT: The postspinel mineral MgAl$_2$O$_4$ exists only under the severe pressure conditions in the subducted oceanic lithosphere in the Earth's deep interior. Here we report that its analogous oxide CdRh$_2$O$_4$ exhibits a structural transition to a quenchable postspinel phase under a high pressure of 6 GPa at 1400 °C, which is within the general pressure range of a conventional single-stage multianvil system. In addition, the complex magnetic contributions to the lattice and metal nonstoichiometry that often complicate investigations of other analogues of MgAl$_2$O$_4$ are absent in CdRh$_2$O$_4$. X-ray crystallography revealed that this postspinel phase has an orthorhombic CaFe$_2$O$_4$ structure, thus making it a practical analogue for investigations into the geophysical role of postspinel MgAl$_2$O$_4$. Replacement of Mg^{2+} with Cd^{2+} appears to be effective in lowering the pressure required for transition, as was suggested for CdGeO$_3$. In addition, Rh^{3+} could also contribute to this reduction, as many analogous Rh oxides of aluminous and silicic minerals have been quenched from lower-pressure conditions.
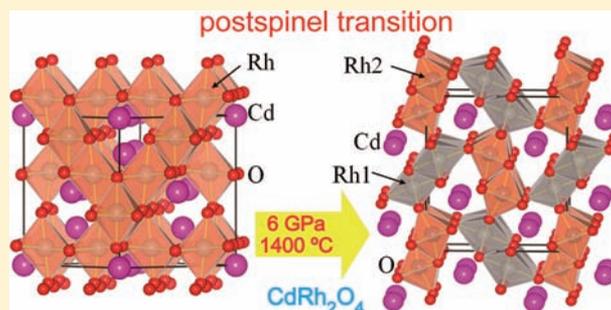
INTRODUCTION

Olivine [(Mg,Fe)$_2$SiO$_4$] is an abundant mineral in the upper mantle and is believed to exhibit a sequence of transitions in crystal structure with depth.[1−3] Each transition leads to a gain in crystal density and is argued to be responsible for the seismic discontinuities observed in the mantle.[4−7] Indeed, experimental and theoretical studies indicate that olivine transforms to a spinel at 18 GPa and 1500 °C and sequentially decomposes into the perovskite (Mg,Fe)SiO$_3$ and the periclase (Mg,Fe)O at 23 GPa and 1600 °C.[8−10] The decomposition is probably responsible for the 660 km discontinuity, which has been detected to separate Earth's upper and lower mantle in underside reflections of shear wave.[11] In addition, aluminous minerals closely related to the spinel MgAl$_2$O$_4$ coexist (∼20% in volume) with silicic materials in the subducted midocean-ridge basalt in the oceanic lithosphere.[12−15] Thus, it is widely accepted that investigations on these aluminous minerals, in addition to the silicic materials, are indispensable to a better understanding of the nature of the lithosphere and the lower mantle.[16]

In studies on the aluminous minerals, the postspinel transition in MgAl$_2$O$_4$ has been identified as being probably the most significant phenomenon in the geophysical role.[17−21] It, however, only occurs at extreme conditions (>25 GPa) that cannot be easily reproduced in the lab. In fact, even the denser morphology of the spinel MgAl$_2$O$_4$ is still poorly understood, although it is quenchable to ambient conditions.[17,19] Thus, it is necessary to identify systems that exhibit analogous transitions under more practical conditions.

Promisingly, recent studies have indicated that there are several oxides besides MgAl$_2$O$_4$ that also undergo a transition from spinel to a CaFe$_2$O$_4$-type structure (Table 1).[22−28] For example, postspinel CuRh$_2$O$_4$,[22] Li$_{0.92}$Mn$_2$O$_4$,[23] and CdCr$_2$O$_4$[24] can be quenched from remarkably low pressures. The quenchable postspinel CuRh$_2$O$_4$, however, shows an additional structural distortion, probably caused by the Jahn−Teller effect of Cu^{2+}, resulting in it belonging to the space group $P2_12_12_1$ rather than $Pnma$. In addition, Li$_{0.92}$Mn$_2$O$_4$ shows a super-

Table 1. Brief Summary of Conditions for Transition from Spinel to a CaFe$_2$O$_4$-Type Structure of MgAl$_2$O$_4$ and Analogous Oxides

| compound | transition condition | | experimental method | r_A/r_B | K_{AB}[a] | space group and lattice parameters | ref. |
	P /GPa	T /°C					
						Quenchable Postspinel	
CdRh$_2$O$_4$	6	1400	XRD	1.426	0.13538	*Pnma* a = 9.12018(8) Å b = 3.05649(3) Å c = 10.7850(1) Å	this study
MgAl$_2$O$_4$	25	1000	XRD	1.294	0.14539	*Pnam* a = 8.631(3) Å[b] b = 9.969(3) Å c = 2.789(1) Å	21
CuRh$_2$O$_4$	4	900	XRD	1.0588	0.18237	*P2$_1$2$_1$2$_1$* a = 3.076(1) Å b = 9.100(1) Å c = 10.571(1) Å	22
Li$_{0.92}$Mn$_2$O$_4$	6	1100	XRD	1.0303 ~1.1333	0.1148 ~0.1182	*Pnma* a = 8.8336(5) Å b = 2.83387(18) Å c = 10.6535(7) Å	23
CdCr$_2$O$_4$	10	1100	XRD	1.5397	0.14892	*Pnam* a = 9.0868(1) Å b = 10.6242(1) Å c = 2.9453(1) Å	24
CoFe$_2$O$_4$	32.5	R.T.[c]	Raman	1.125	0.20423	*Pnma* a = 9.483(21) Å b = 2.959(12) Å c = 10.401(20) Å	25
CaAl$_2$O$_4$[d]	10	1100	XRD	1.941	0.10448	*Pnam* a = 8.92004(5) Å b = 10.31550(6) Å c = 2.87129(1) Å	26
ZnFe$_2$O$_4$	24.6~34.2	R.T.	Raman	1.156	0.19751		18
						Unquenchable Postspinel	
MgCr$_2$O$_4$	14.2~30.1	R.T.	Raman	1.048	0.14542		27
ZnCr$_2$O$_4$	17.5~35	R.T.	Raman	1.175	0.18877		28

[a]$K_{AB} = X_A X_B/r_e^2$, where $r_e^2 = (r_A + r_O)^2 + (r_B + r_O)^2 + 1.155(r_A + r_O)(r_B + r_O)$; $X_A (X_B)$ is the electronegativity of the $A(B)$ ion; and r_A, r_B, and r_O are the effective radii of A, B, and O ions, respectively. [b]Measured at 25 GPa and 1000 °C. [c]Room temperature. [d]An intermediate structure ($P2_1/m$) appears between the spinel and the CaFe$_2$O$_4$-type structures.[26]

structure due to ordering of Li-vacancies,[23] and CdCr$_2$O$_4$ shows multiple anomalies in specific heat, which have been suggested to be associated with complex magnetic transitions.[24] Thus, a better analogue is required that does not have additional contributions to the lattice from magnetism and metal nonstoichiometry.

Note that other major postspinel structures of CaTi$_2$O$_4$-type (*Bbmm*) and CaMn$_2$O$_4$-type (*Pmab*) have substantial magnetic contributions to the lattice, including the Jahn−Teller distortion.[26]

Recently, we focused our attention on the spinel oxide CdRh$_2$O$_4$, which crystallizes into a cubic structure (*Fd$\bar{3}$m*, a = 8.73 Å),[29] because its analogous Rh^{3+} oxides have a bandgap of 2.1−2.74 eV, which makes it promising as a transparent semiconductor.[30] Octahedral coordination of Rh^{3+} (4d^6) leads to d-orbital splitting into fully occupied t$_{2g}^6$ and empty e$_g^0$ levels. Thus motivated, we initially began a high-pressure and high-temperature study of CdRh$_2$O$_4$ to control the electrical and magnetic properties over a wide range via doping. However, during the course of our study, we found that CdRh$_2$O$_4$ undergoes a structural transition from the spinel to

an orthorhombic structure at 6 GPa and 1400 °C. Crystal structure analysis identified that the quenched orthorhombic structure is of the CaFe$_2$O$_4$ type and the calculated crystal density appeared to increase by 10.1% after transition. This transition thus can be considered as an analogous postspinel transition that occurs in the general pressure range of a single-stage anvil system. This would make the material very practical for geophysical studies. Here we report the crystal structure and the magnetic and electronic properties of the postspinel CdRh$_2$O$_4$. We show that it is cation stoichiometric and remains nonmagnetic even after the transition. Thus, quenched CdRh$_2$O$_4$ should be useful in probing the nature of the postspinel transition of MgAl$_2$O$_4$.

■ EXPERIMENTAL SECTION

A polycrystalline pellet of postspinel CdRh$_2$O$_4$ was prepared by means of a solid-state reaction from powders of CdO (99.99%, Wako Chem.) and Rh$_2$O$_3$. The precursor Rh$_2$O$_3$ was prepared from Rh powder (99.9%, Western Platinum Ltd.) by heating at 900 °C in oxygen for 24 h. A stoichiometric mixture of CdO and Rh$_2$O$_3$ was sealed into an Au capsule, which was set into a belt-type high-pressure apparatus capable of maintaining 6 GPa during heating at 1400 °C for 1 h. The capsule

was then quenched to ambient temperature before releasing the pressure. The final product was dense and black in color.

For comparison, a polycrystalline pellet of $CdRh_2O_4$ was prepared without applying pressure during heating by a comparable method. A stoichiometric mixture of CdO and Rh_2O_3 was heated at 900 °C in air for 3 days with several intermediate grindings. The final product was a dense pellet and approximately reddish-brown in color.

The products were investigated by powder X-ray diffraction (XRD) at room temperature using monochromatic Cu-Kα radiation from a commercial diffractometer (RIGAKU RINT 2500). The data were collected in a 2θ range from 10° to 110° in steps of 0.02°. The counting time was 10 s per step and the X-ray tube was operated at 40 kV and 300 mA. The crystal structure was analyzed by the Rietveld method using the program RIETAN-FP.[31] The XRD pattern revealed 0.36 mass% of Rh metal in the high-pressure synthesized pellet and 2.73 mass% in the pellet prepared without the high pressure, suggesting a slight off-stoichiometry for both the pellets. Despite repeated attempts, however, the amount of Rh metal was not diminished.

The oxygen content of each pellet was measured by a thermogravimetric (TG) method on a TGA-1 from PerkinElmer at a heating rate of 2 °C/min in 5% hydrogen/argon. Saturated weight loss was clearly observed at 240 °C after 1 h of heating; the measurement was repeated three times for each pellet. On the assumption that the samples are cation stoichiometric, the average weight loss indicates that the oxygen content is 3.92(1) and 4.02(4) per formula unit for the samples prepared with and without the high pressure, respectively. The TG analysis suggested that some oxygen vacancies were introduced in the high-pressure sample.

Magnetic susceptibility (χ) was measured in a Magnetic Property Measurement System from Quantum Design at temperatures between 2 and 350 K in an applied magnetic field of 10 kOe under field-cooling (FC) and zero-field-cooling (ZFC) conditions. Isothermal magnetization between −50 kOe and 50 kOe was recorded at temperatures of 2 and 300 K with the same apparatus. A Physical Properties Measurement System from Quantum Design was used to measure the electrical resistivity (ρ) of the polycrystalline pellets at temperatures between 2 and 300 K upon cooling and heating by a four-terminal method with a dc-gauge current of 5 μA. Specific heat (C_p) measurements were conducted on the same apparatus at temperatures between 2 and 300 K upon cooling by a quasi-adiabatic method. Note that each pellet was carefully polished to remove the surface contaminants prior to the measurements mentioned above.

RESULTS

The XRD pattern for the spinel was refined by using the structure model proposed in ref 29, resulting in a reasonable solution (Figure 1a). The spinel $CaRh_2O_4$ appears to crystallize in a diamond-type structure belonging to the space group $Fd\bar{3}m$. Because the solution does not revise the crystallographic data,[29] details of the spinel structure are not fully described here (shown in the Supporting Information). Briefly, our results on the spinel were as follows: the R factors of the final solution, R_{wp} and R_p were 7.29% and 5.07%, respectively, and the goodness of fit S was 1.72,[32] confirming that the $Fd\bar{3}m$ structure model reasonably fits the present compound. Refinement yielded lattice parameters a of 8.722(2) Å and V of 663.4(3) Å^3, which are in agreement with previous results.

The analysis indicates that 2.73 mass% of Rh metal coexists with the spinel $CdRh_2O_4$ in the final product, suggesting a possible metal defect in the spinel. To test the possibility, the site occupancies of the metal atoms were investigated while analyzing the XRD pattern. However, a refinement indicated that the each metal site was fully occupied. Thus, the structural parameters were unrefined in the final step (fixed to 1). In the final refinement, we found that the average Rh−O distance is 2.049 (1) Å and the Cd−O distance is 2.133(3) Å, leading to a
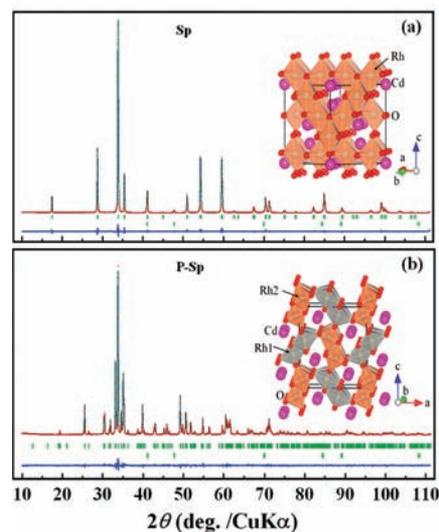
Figure 1. (a) XRD pattern of the spinel (Sp) and (b) postspinel (P-Sp) $CdRh_2O_4$ at ambient conditions. The patterns were analyzed by a Rietveld method. Markers and solid lines show the observed and the calculated profiles, respectively, and the difference between those is shown at the bottom. Bragg positions are marked by small ticks (upper and lower lines for $CdRh_2O_4$ and Rh, respectively). The corresponding schematic crystal structure is shown in the inset.

bond valence sum (BVS)[33,34] of 2.99 for Rh and 2.15 for Cd. The BVS indicates that the structure model can be reasonable even without the defects. Note that the oxygen occupancy factors were also investigated. Oxygen nonstoichiometry was however not suggested in the refinements. This accords well with the TG result [4.02(4) moles of oxygen per the formula unit]. Thus, the oxygen-occupancy factor was fixed to 1, as were the other occupancy factors in the final refinement.

Next, we analyzed the crystal structure of the $CdRh_2O_4$ quenched from the high-pressure condition. We see that the XRD pattern (Figure 1b) is entirely different from the spinel profile, suggesting a major structure transition. Detailed Rietveld analysis indicated that the quenched structure is well described by the $CaFe_2O_4$-type structure model as well as the structure of $CaRh_2O_4$.[35] The orthorhombic unit cell with the space group of $Pnma$ with lattice constants a = 9.12018(8) Å, b = 3.05649(3) Å, and c = 10.7850(1) Å was found for the postspinel $CdRh_2O_4$. The R factors of the solution were below 6.9%, suggesting a good quality. See Tables 2 and 3 for a summary of the structural parameters and selected bond distances and angles, respectively. Note that tiny reflections from Rh metal were detected in the analysis (0.36 mass%). However, refinements of the variable site occupancies for metals suggested that Rh and Cd vacancies were at undetectable levels. We believe that the trivial amount of Rh metal stems from slight off-stoichiometry of the starting mixtures.

The schematic structural view (b-axis projection) shown in the insets to Figures 1a and 1b, drawn based on the refined results, indicate a structure that is highly similar to $CaFe_2O_4$: Rh^{3+} atoms occupy two crystallographic sites (Rh1 and Rh2), which are coordinated by six O atoms each. The neighboring Rh1-O_6 and Rh2-O_6 octahedra share edges and corners as shown in Figure 2, forming a hollandite-like cage running along the b-axis; all Cd^{2+} ions reside in this cage. The structural

Table 2. Atomic Coordinates, Isotropic Displacement Parameters, and Crystallographic Data of the Postspinel $CdRh_2O_4$.

formula	$CdRh_2O_4$
formula weight	382.22
temperature	R.T.
wavelength	1.540593Å $(CuK_{\alpha1})$
space group	$Pnma$ (No.62)
lattice constants	a = 9.12018(8) Å, b = 3.05649(3) Å, c = 10.7850(1) Å, V = 300.639(5) Å³
Z	4
calculated density	8.425 g/cm³
R-factors	R_{wp} = 6.882%, R_p = 5.280%, R_B = 1.618%, R_F = 1.041%, $S = R_{wp}/R_e$ = 1.2116
refinement software	RIETAN-FP

atom	site	x	y	z	g	B (Å²)
Cd	$4c$	0.7653(1)	0.25	0.66214(9)	1	1.21(3)
Rh1	$4c$	0.4069(1)	0.25	0.09804(9)	1	0.83(2)
Rh2	$4c$	0.4484(1)	0.25	0.61662(9)	1	0.90(3)
O1	$4c$	0.1966(8)	0.25	0.1680(8)	0.971(16)	0.7(2)
O2	$4c$	0.1160(7)	0.25	0.4715(7)	1	0.6(2)
O3	$4c$	0.5459(8)	0.25	0.7848(7)	1	1.0(2)
O4	$4c$	0.4089(8)	0.25	0.4332(8)	0.972(16)	1.4(2)

Table 3. Selected Bond Distances, Bond Angles, and BVS of Postspinel $CdRh_2O_4$

atoms		distances(Å)	atoms	angles(deg.)
Cd	O1×2	2.411(6)	Rh1−O2−Rh1	98.5(3)
	O2×2	2.363(6)	Rh1−O2−Rh1	95.8(3)
	O3	2.398(8)	Rh1−O3−Rh1	97.7(3)
	O3	2.623(8)	Rh1−O1−Rh2	119.4(3)
	O4×2	2.433(5)	Rh2−O1−Rh2	93.7(3)
Rh1	O1	2.062(8)	Rh2−O3−Rh1	130.7(2)
	O2	2.060(5)	Rh2−O4−Rh2	98.2(2)
	O2×2	2.049(6)	Rh2−O4−Rh2	94.7(3)
	O3×2	2.029(5)		
Rh2	O1×2	2.096(5)	BVS(Cd)	1.97
	O3	2.020(8)	BVS(Rh1)	3.00
	O4	2.011(7)	BVS(Rh2)	2.89
	O4×2	2.078(5)		
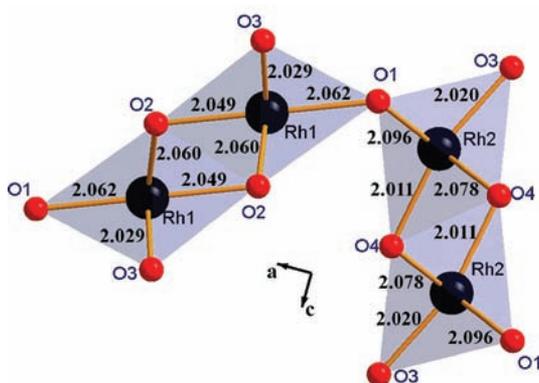
Figure 2. Local coordination of Rh in the postspinel structure. Numbers indicate the bond distances in the units of angstrom. The bond angles are shown in Table 3.

features are also similar to the postspinel oxides $Li_{0.92}Mn_2O_4$,[23] $NaRh_2O_4$,[35] and $CdCr_2O_4$.[24]

TG analysis indicated possible oxygen nonstoichiometry [3.92(1) moles of oxygen per formula unit] for the quenched $CdRh_2O_4$; thus, we tried to refine the oxygen quantity in the analysis. The oxygen site occupancies of O1, O2, O3, and O4 were tested and O1 and O4 were refined to be 0.971(16) and 0.972(16), respectively. Meanwhile, the O2 and O3 site occupancies were found to be slightly larger than 1, and so were fixed at 1 in the final step. Thus, the average oxygen quantity was 3.94, which is comparable to the TG estimate. Note that O1 and O4 are bonded to Rh2. Besides, the thermal displacement parameters and BVS were investigated. The thermal displacement parameters in Table 2 are neither unusually large nor small. The BVS values are 3.00 for Rh1, 2.89 for Rh2, and 1.97 for Cd, indicating good agreement with the expectation. We conclude that the fraction of vacancies at the oxygen sites is no higher than 3%. The site preference of the oxygen vacancies is, however, not understood, and the future use of neutron diffraction may clarify the issue.

From the magnetic property measurements (Figure 3a), we found that the spinel has an almost temperature-independent χ,
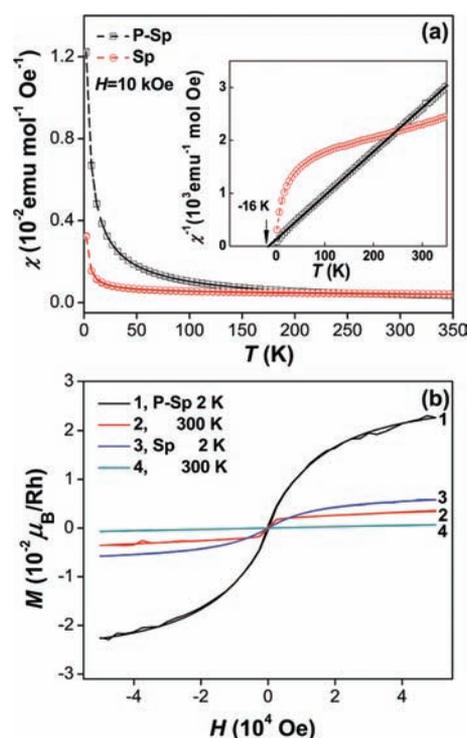
Figure 3. (a) T dependence of χ for the spinel and postspinel $CdRh_2O_4$. Inset shows T dependence of the inverse χ. (b) Isothermal magnetization of the spinel and postspinel $CdRh_2O_4$ at temperatures of 2 and 300 K.

as expected from the nonmagnetic electronic configuration of Rh^{3+} (4d⁶: $t_{2g}^6 e_g^0$, S = 0). The small upturn below approximately 20 K is likely an impurity contribution. Meanwhile, the postspinel shows slight temperature dependence in χ, although the electronic configuration of Rh^{3+} is unaltered formally. The thermal hysteresis between the ZFC and FC curves is not obvious for both the compounds over the temperature range. To analyze the magnetic features further, we applied the Curie−Weiss law to the postspinel data in the temperature range between 40 and 350 K (see the solid line in the inset to Figure 3a):

$$\chi^{-1} = 3\pi N_A^{-1} \mu^{-2}_{\text{eff}} (T - \Theta_W)$$

where μ_{eff} is the effective Bohr magneton, N_A is the Avogadro constant, and Θ_W is the Weiss temperature. The analysis yielded a μ_{eff} of 0.064 μ_B/Rh and a Θ_W of -16 K, suggesting that the magnetic moment is fairly small on average and the magnetic moments have weakly antiferromagnetic interaction. Although the source of the magnetic moments is not yet clear, the most probable source is the small amount of Rh^{2+} ($4d^7$: t^6_{2g} e^1_g, $S = 1/2$) distributed among the nonmagnetic Rh^{3+} to compensate for the charge unbalance caused by the small number of the oxygen vacancies. Alternatively, possible hybridization of the 4d orbital over the edge-shared RhO_6 octahedra may account for the magnetic features to some extent. Further study to determining the origin of this slight magnetic activation is in progress.

As shown in Figure 3b, magnetic hysteresis was not detected in isothermal magnetization measurements at 2 and 300 K. Even the largest magnetization of 0.023 μ_B/Rh at 2 K (50 kOe; the postspinel) was just 2% of the full magnetization of Rh^{2+}, indicating the observed magnetic moments are indeed trivial.

We also compared the temperature dependence of ρ for the spinel and postspinel $CdRh_2O_4$, as shown in Figure 4a. Note
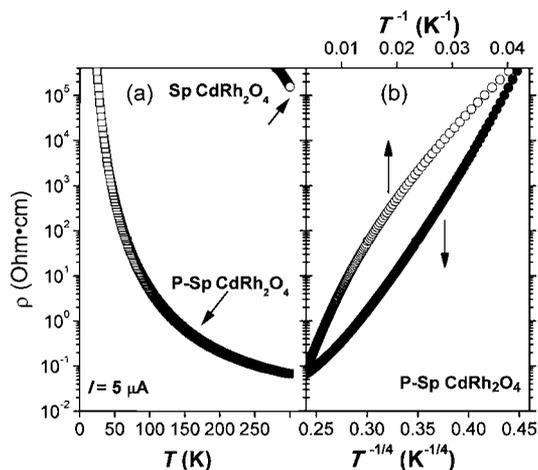
Figure 4. (a) T dependence of ρ for the spinel and postspinel $CdRh_2O_4$. (b) The postspinel data are plotted in the Arrhenius (ρ vs T^{-1}) and the variable range hopping (ρ vs $T^{-1/4}$) forms for a comparison.

that the ρ of the spinel and postspinel go beyond the instrumental limit on cooling to ~280 K and ~22 K, respectively. The temperature dependence of ρ for both the compounds is primarily characterized by a negative slope $d\rho/dT < 0$, indicating semiconductor-like characteristics. The results probably reflect the fundamental electronic gap between the fully filled t_{2g} and the empty e_g levels. Rough estimates of the activation energy E_a obtained by Arrhenius analysis with the following formula were >2 eV for the spinel and 0.50 eV for the postspinel, respectively: $\rho^{-1}(T) = (A/T) \exp(-E_a/k_B T)$, where A is a constant and k_B is the Boltzmann constant.[36,37] The quantitative difference in the gaps may reflect a major change of the electronic structure caused by the structural transition.

To further analyze the semiconductor-like features of the postspinel, the data (22 K−300 K) were plotted to fit two alternative conduction models (Figure 4b): Arrhenius (ρ vs $1/T$) and variable range hopping (VRH; ρ vs $1/T^{1/4}$). It appears that neither plot follows a single line, indicating that neither

conduction model sufficiently accounts for the observed conduction. Perhaps complex conduction across grain boundaries and surfaces may be somewhat involved in the observed charge transport.

To further investigate the electronic properties, we measured C_p for both compounds for temperatures between 2 and 300 K. As shown in Figures 5a and 5b, both compounds have a
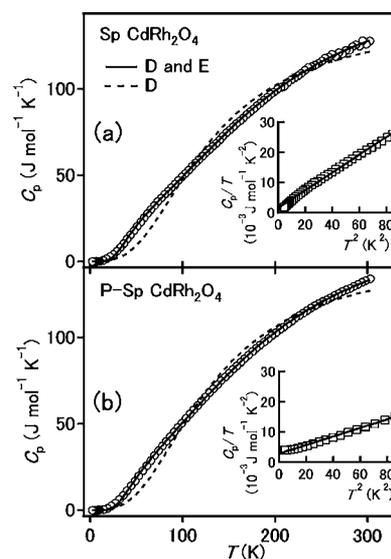
Figure 5. C_p vs T and a low-temperature portion of C_p/T vs T^2 for (a) the spinel and (b) postspinel $CdRh_2O_4$. Solid curve depicts fitting to the data by a linear combination of the Debye and the Einstein models (D and E). The broken curve was achieved only by the D model. Solid line in the inset each depicts fitting by the approximated D model.

continuous and monotonic temperature dependence of C_p. No anomalous features are obvious, showing that no major phase transitions take place in this temperature range. The plot of C_p vs T was quantitatively analyzed by using a linear combination of the Debye model and the Einstein model as well as that for KOs_2O_6 and $RbOs_2O_6$.[38] The analytical formula is

$$C(T) = n_D \times 9N_A k_B \left(\frac{T}{T_D}\right)^3 \int_0^{T_D/T} \frac{x^4 e^x}{(e^x - 1)^2} dx$$

$$+ n_E \times 3N_A k_B \left(\frac{T_E}{T}\right)^2 \frac{e^{T_E/T}}{(e^{T_E/T} - 1)^2},$$

where N_A is Avogadro's constant; k_B is the Boltzmann's constant; and T_D and T_E are the Debye and the Einstein temperatures, respectively. The scale factors n_D and n_E correspond to the numbers of vibrating modes per formula unit in the Debye and Einstein models, respectively. Fitting to the curves yields T_D of 840(6) K, T_E of 165(2) K, n_D of 4.95(2), and n_E of 1.71(3) for the spinel and T_D of 846(7) K, T_E of 187(2) K, n_D of 5.02(2), and n_E of 1.90(3) for the postspinel (see the solid curves in Figures 5a and 5b). No essential difference can be seen in these sets of thermodynamical parameters. The Einstein term dramatically increases the fitting quality (see the broken curves achieved without the Einstein term), suggesting that the phonon density of states (DOS) at frequencies corresponding to 300 K or below construct a much complex DOS structure than that for Debye model.

The low-temperature part of the C_p/T vs T^2 plot (Figure 5b) is well characterized by a least-squares method using the approximated Debye model $C_v/T = \gamma + 2.4\pi^4 r N_A k_B (1/T_D^3) T^2$, where γ is the electronic term and r is the number of atoms per formula unit (see the solid lines in the insets to Figures 5a and 5b). The analysis yields γ of 1.6(1) mJ mol^{-1} K^{-2} and T_D of 359(1) K for the spinel CdRh$_2$O$_4$ and γ of 2.8(1) mJ mol^{-1} K^{-2} and T_D of 457(3) K for the postspinel CdRh$_2$O$_4$. The small γ observed for both indicates a small DOS at the Fermi level (E_F), possibly introduced by the small amount of oxygen vacancies. This small DOS may be implicated in the temperature dependence of χ and the complicated hopping conduction. The increase in T_D probably corresponds to increased hardness of the lattice caused by the density increase via the structure transition. Further study of the elasticity properties of the compounds may enable a more precise analysis of the increase in T_D.

Finally, electronic state of the spinel and postspinel CdRh$_2$O$_4$ was investigated by a first-principles method. As shown in Figures 6a and 6b, the DOS of the spinel and postspinel
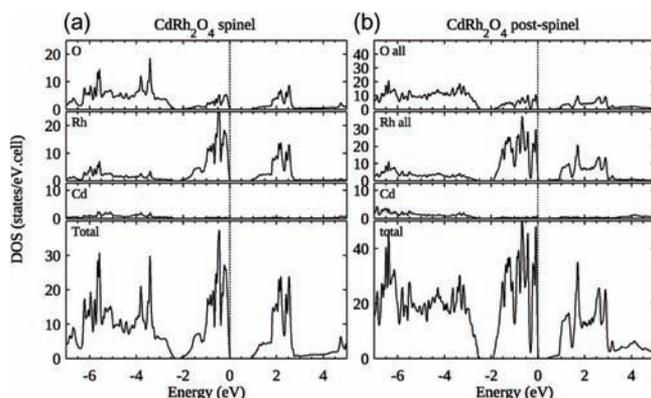
Figure 6. Total and partial densities of states (DOS) for (a) the spinel and (b) postspinel CdRh$_2$O$_4$.

CdRh$_2$O$_4$ were calculated by the local-density approximation (LDA) method based on density functional theory.[39] The WIEN2K package, which is based on the highly precise full-potential linearized augmented-plane-wave method, was used.[40] The Rh 4d states of the spinel and postspinel CdRh$_2$O$_4$ are split into the fully occupied t$_{2g}$ and the empty e$_g$ bands. Each stoichiometric compound is thus expected to have a certain energy gap at the E_F level. This primarily accounts for the observed electrically insulating features for the spinel and postspinel CdRh$_2$O$_4$ and suggests that the nonzero γ detected in the C_p measurements is most likely due to a small amount of charged carries doped by nonstoichiometry.

The DOS structure nearby the E_F level of the postspinel is higher and sharper than that of the spinel; thus hole carriers introduced by methods such as a chemical doping possibly results in electronic instability, which often produces remarkable electromagnetic properties. Chemical doping to the postspinel CdRh$_2$O$_4$ has been attempted to develop electromagnetic properties further under the high-pressure and temperature condition.

■ DISCUSSION AND CONCLUSIONS

The present results for CdRh$_2$O$_4$ and previous results for CdGeO$_3$[41] suggest that replacement of Mg^{2+} with Cd^{2+} is likely effective in lowering the pressure required for structural

transition in aluminous and silicic minerals. In fact, CdGeO$_3$ shows analogous sequential transitions below 10 GPa, which was also found for MgSiO$_3$.[41] The practical synthesis conditions and promising characteristics probably stem from a delicate balance between ionic size and local coordination features for both Mg and Cd. Although we do not fully understand the role of the replacement, it likely provides better opportunities for analogous studies in geophysical science. For example, a transition from CaFe$_2$O$_4$-type to a much denser structure has been suggested for a mineral postspinel in crust.[42] The required pressure condition is however too severe to experimentally confirm the possible "post-postspinel" transition in minerals. Analogous oxides are practically helpful to test the possibility.

Furthermore, many analogous Rh oxides of aluminous and silicic minerals have been discovered thus far, including CaRhO$_3$ (perovskite[43] and postperovskite[44,45]), RhO$_2$ (rutile[46] and CaCl$_2$-type[46]), Rh$_2$O$_3$ (corundum[47,48] and Rh$_2$O$_3$(II)-type[48]), CaRh$_2$O$_4$ (postspinel[35]), Bi$_{0.68}$Be$_2$Rh$_6$O$_{12}$ (NAL phase[49]), Ba$_{1.72}$Rh$_8$O$_{16}$ (hollandite[50]). The present compound, CdRh$_2$O$_4$, is a unique member of the Rh family in that it undergoes a spinel-to-CaFe$_2$O$_4$ transformation that is analogous to what was found for MgAl$_2$O$_4$. Note that CuRh$_2$O$_4$ shows a similar transformation under the influence of Jahn−Teller distortion, resulting in a different space group (see Table 1) from that of MgAl$_2$O$_4$.[22]

The structural transition leads to a remarkable increase in the crystal density of 10.1% from 7.65 g/cm^3 for the spinel, which is comparable to what was quantitatively found for analogous oxides such as CdCr$_2$O$_4$ (10.6%[24]) and MgAl$_2$O$_4$ (10.03%[21]). The mechanism in ref 24 probably operates to explain the density differences: the cation displacement and full octahedral movement under the high-pressure and high-temperature condition may explain the density increase.

As previously discussed by Kugimiya and Steinfink (KS),[51] two principle parameters may categorize the structure types of AB_2O_4 compounds: the ionic size ratio r_A/r_B and the bond stretching constant $K_{AB} = X_A X_B/r_e^2$, where $r_e^2 = (r_A + r_O)^2 + (r_B + r_O)^2 + 1.155(r_A + r_O)(r_B + r_O)$; r_A, r_B, and r_O are the effective radii of A, B, and O, respectively; and X_A and X_B are the electronegativities of the A and B atoms, respectively.[51] We set $r_{Cd}^{2+} = 0.97$ Å, $r_{Rh}^{3+} = 0.68$ Å, $r_O^{2-} = 1.40$ Å, $X_{Cd} = 1.46$, and $X_{Rh} = 1.45$, which yielded $K_{AB} = 0.13538$ and $r_A/r_B = 1.426$ for the postspinel CdRh$_2$O$_4$.[51,52] Within the KS scheme, the structure of CdRh$_2$O$_4$ is categorized as being of the CaFe$_2$O$_4$ type ($0.9<r_A/r_B < 1.7$ and $0.04<K_{AB} < 0.18$). However, it actually crystallizes into a spinel structure at ambient pressure. Conversely, CoFe$_2$O$_4$ ($K_{AB} = 0.2042$; see Table 1), ZnFe$_2$O$_4$ (0.1975), ZnCr$_2$O$_4$ (0.1887), and CuRh$_2$O$_4$ (0.2042) are slightly out of the range of the CaFe$_2$O$_4$ type, although they actually crystallize into the CaFe$_2$O$_4$-type structure under certain pressures. All of these compounds contain a 3d element at the A-site in AB_2O_4, implying a possible need to revise the KS scheme, which was proposed in 1968. Moreover, we have tried to synthesize additional postspinel oxides using the KS scheme; unfortunately, our attempts thus far have been unsuccessful. We are actually unable to predict that the CaFe$_2$O$_4$-type AB_2O_4 is either quenchable or unquenchable from a high-pressure condition. Further improvement of the scheme may help to predict the structural stability of the postspinel oxides.

In summary, we successfully quenched a postspinel phase of CdRh$_2$O$_4$ from 6 GPa and 1400 °C to ambient conditions. This indicates that the spinel-to-CaFe$_2$O$_4$-type structure transition

takes place in the general range pressures possible with a single-stage high-pressure apparatus such as a multianvil system. Thus, this compound will be helpful as an analogous oxide of the postspinel mineral $MgAl_2O_4$, which only exists under far more severe pressure conditions in the Earth's deep interior. In addition, the postspinel remains nonmagnetic across the transition, which is beneficial for geophysical studies because complex magnetic contributions to the lattice are absent. Moreover, it is cation stoichiometric, unlike $Li_{0.92}Mn_2O_4$, making it helpful for a first-principles study. Besides, much sharper and higher DOS structure of the postspinel phase rather than that of the spinel phase nearby the E_F level was suggested in the theoretical study: electromagnetic properties beyond those of the doped spinel phase are potentially developed further by hole carriers doping. Because a single-crystal of an analogous postspinel oxide is of particular interest not only in geophysical science but also in materials science, growth of single-crystals of the postspinel $CdRh_2O_4$ certainly should be attempted, as it was successful for $CaRh_2O_4$ [35] and NaV_2O_4 [53] under comparable high-pressure conditions. Attempts to dope hole carries to the postspinel $CdRh_2O_4$ and to grow a high-quality single-crystal are in progress.

ASSOCIATED CONTENT

Supporting Information

Crystallographic data in CIF format. Further details are given in Tables S1 and S2. This material is available free of charge via the Internet at http://pubs.acs.org.

AUTHOR INFORMATION

Corresponding Author
*E-mail: guo.yanfeng@nims.go.jp (Y.G.); yamaura.kazunari@nims.go.jp (K.Y.).

Notes

The authors declare no competing financial interest.

ACKNOWLEDGMENTS

REFERENCES

(1) Ringwood, A. E. *Geochim. Cosmochim. Acta* **1991**, *55*, 2083.
(2) Weidner, D. J. In *Chemistry and Physics of Terrestrial Planets*; Saxena, S. K., Ed.; Springer-Verlag: New York, 1986; pp 251−274.
(3) Jackson, I. *Earth Planet. Sci. Lett.* **1983**, *62*, 91.
(4) Helffrich, G. *Rev. Geophys.* **2000**, *38*, 141.
(5) Ito, E.; Akaogi, M.; Topor, I.; Navrotsky, A. *Science* **1990**, *249*, 1275.
(6) Ito, E.; Takahashi, E. J. *Geophys. Res.* **1989**, *94*, 10637.
(7) Liu, L.-G. *Geophys. Res. Lett.* **1975**, *2*, 417.
(8) Liu, L. *Nature* **1976**, *262*, 770.
(9) Akimoto, S.; Fujisawa, J. *Geophys. Res.* **1968**, *73*, 1467.
(10) Ringwood, A. E.; Major, A. *Earth Planet. Sci. Lett.* **1966**, *1*, 241.
(11) Deuss, A.; Redfern, S. A. T.; Chambers, K.; Woodhouse, J. H. *Science* **2006**, *311*, 198.
(12) Ono, S.; Ito, E.; Katsura, T. *Earth Planet. Sci.* **2001**, *190*, 57.
(13) Hirose, K.; Fei, Y.; Ma, Y.; Mao, H. K. *Nature* **1999**, *397*, 53.
(14) Kesson, S. E.; Fitzgerald, J. D.; Shelley, J. M. G. *Nature* **1994**, *372*, 767.
(15) Irifune, T.; Ringwood, A. E. *Earth Planet. Sci.* **1993**, *117*, 101.
(16) Akaogi, M. *Geol. Soc. Am. Bull.* **2007**, *421*, 1.
(17) Kojitani, H.; Enomoto, A.; Tsukamoto, S.; Akaogi, M.; Miura, H.; Yusa, H. *J. Phys: Conf. Ser.* **2010**, *215*, 012098.
(18) Wang, Z.; Schiferl, D.; Zhao, Y.; O'Neill, H. S. C. *J. Phys. Chem. Solids* **2003**, *64*, 2517.
(19) Irifune, T.; Naka, H.; Sanehira, T.; Inoue, T.; Funakoshi, K. *Phys. Chem. Miner.* **2002**, *29*, 645.
(20) Catti, M. *Phys. Chem. Miner.* **2001**, *8*, 729.
(21) Irifune, T.; Fujino, K.; Ohtani, E. *Nature* **1991**, *349*, 409.
(22) Ohgushi, K.; Gotou, H.; Yagi, T.; Ueda, Y. *J. Phys. Soc. Jpn.* **2006**, *75*, 023707.
(23) Yamaura, K.; Huang, Q.; Zhang, L.; Takada, K.; Baba, Y.; Nagai, T.; Matsui, Y.; Kosuda, K.; Takayama-Muromachi, E. *J. Am. Chem. Soc.* **2006**, *128*, 9448.
(24) Arevalo-Lopez, A. M.; Dos Santos-Gacia, A. J.; Castillo-Martinez, E.; Duran, A.; Alario-Franco, M. A. *Inorg. Chem.* **2010**, *49*, 2827.
(25) Wang, Z.; Downs, R. T.; Pischedda, V.; Shetty, R.; Saxena, S. K.; Zha, C. S.; Zhao, Y. S.; Shciferl, D.; Waskowska, A. *Phys. Rev. B* **2003**, *68*, 094101.
(26) Lazić, B.; Kahlenberg, V.; Konzett, J.; Kaindl, R. *Solid State Sci.* **2006**, *8*, 589.
(27) Wang, Z.; O'Neill, H. S. C.; Lazor, P.; Saxena, S. K. *J. Phys. Chem. Solids* **2002**, *63*, 2057.
(28) Wang, Z.; Lazor, P.; Saxena, S. K. J.; Artioli, G. *J. Solid State Chem.* **2002**, *165*, 165.
(29) Agarwala, R. P. Z. *Anorg. Chem.* **1961**, *307*, 205.
(30) Mizoguchi, H.; Hirano, M.; Fujitsu, S.; Takeuchi, T.; Ueda, K.; Hosono, H. *Appl. Phys. Lett.* **2002**, *80*, 1207.
(31) Izumi, F.; Momma, K. *Solid State Phenom.* **2007**, *130*, 15.
(32) Young, R. A. *The Rietveld Method*; Young, R. A., Ed.; Oxford University Press: Oxford, U.K., 1993.
(33) Brown, I. D. *Acta Crystallogr., Sect. B* **1977**, *33*, 1305.
(34) Yamaura, J.; Yonezawa, S.; Muraoka, Y.; Hiroi, Z. *J. Solid State Chem.* **2006**, *179*, 336.
(35) Yamaura, K.; Huang, Q.; Moldovan, M.; Young, D. P.; Sato, A.; Baba, Y.; Nagai, T.; Matsui, Y.; Takayama-Muromachi, E. *Chem. Mater.* **2005**, *17*, 359.
(36) Tuller, H. L.; Nowick, A. S. *J. Phys. Chem. Solids* **1977**, *38*, 859.
(37) Perdew, J. P.; Wang, Y. *Phys. Rev. B* **1992**, *45*, 13244.
(38) Bruhwiler, M.; Kazakov, S. M.; Zhigadlo, N. D.; Karpinski., J.; Batlogg, B. *Phys. Rev. B* **2004**, *70*, 020503R.
(39) Hohenberg, P.; Kohn, W. *Phys. Rev.* **1964**, *B864*, 136.
(40) Blaha, P.; Schwarz, K.; Madsen, G. K. H.; Kvasnicka, D.; Luitz, J. *WIEN2K: An Augmented Plane Wave+Local orbitals Program for Calculating Crystal Properties*; Karlheinz Schwarz, Tech. Universitat Wien: Wien, Austria, 2001.
(41) Akaogi, M.; Navrotsky, A. *Phys. Chem. Miner.* **1987**, *14*, 435.
(42) Yamanaka, T.; Uchida, A.; Nakamoto, Y. *Am. Mineral.* **2008**, *93*, 1874.
(43) Yamaura, K.; Takayama-Muromachi, E. *Phys. C* **2006**, *445−448*, 54.
(44) Shirako, Y.; Kojitani, H.; Akaogi, M.; Yamaura, K.; Takayama-Muromachi, E. *Phys. Chem. Miner.* **2009**, *36*, 455.
(45) Shirako, Y.; Kojitani, H.; Oganov, A. R.; Fujino, K.; Miura, H.; Mori, D.; Inaguma, Y.; Yamaura, K.; Akaogi, M. *Am. Mineral.* **2012**, *97*, 159.
(46) Shannon, R. D. *Solid State Commun.* **1968**, *6*, 139.
(47) Coey, J. M. D. *Acta Crystallogr.* **1970**, *B26*, 1876.
(48) Shannon, R. D.; Prewitt, C. T. *J. Solid State Chem.* **1969**, *2*, 134.
(49) Mizoguchi, H.; Zakharov, L. N.; Marshall, W. J.; Sleight, A. W.; Subramanian, A. A. *Chem. Mater.* **2009**, *21*, 994.
(50) Siegrist, T.; Larson, E. M.; Chamberland, B. L. *J. Alloys Compd.* **1994**, *210*, 13.
(51) Kugimiya, K.; Steinfink, H. *Inorg. Chem.* **1968**, *7*, 1762.
(52) Shim, S. H.; Duffy, T. S.; Shen, G. Y. *Nature* **2001**, *411*, 571.

(53) Yamaura, K.; Arai, M.; Sato, A.; Karki, A. B.; Young, D. P.; Movshovich, R.; Okamoto, S.; Mandrus, D.; Takayama-Muromachi, E. *Phys. Rev. Lett.* **2007**, *99*, 196601.

6875

dx.doi.org/10.1021/ic300628m | *Inorg. Chem.* 2012, 51, 6868−6875